



Electrostatic Micromotors Supported on Microball Bearings

Nima Ghalichechian, Alireza Modafe, Mustafa Beyaz, Nick Ganing, and Reza Ghodssi

Dept. of Electrical and Computer Engineering, Institute for Systems Research, University of Maryland – College Park, MD 20742, USA

MEMS Sensors and Actuators Laboratory (MSAL)

INTRODUCTION

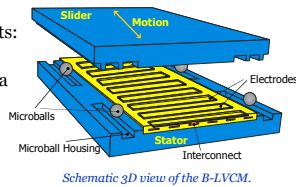
OBJECTIVE: To characterize the dynamic behavior of a bottom-drive, linear, variable-capacitance (B-LVCM) micromotor supported on microball bearings.

- Microball bearing technology in silicon provides a reliable support mechanism for the rotor of micromotors and microgenerators.
- The primary application of the B-LVCM is long-range, high-speed, linear micro-positioning.
- Mechanical properties of roller bearing can be studied by characterization of the B-LVCM.
- B-LVCM is a platform for developing a rotary micromotor.

DESIGN AND FABRICATION

- The micromotor comprises three major components: stator, slider, and microballs.
- Bottom-drive design results in increased active area and increased motor force.
- Six-phase design results in small force ripples.
- Microball bearing design provides a mechanical support for maintaining a uniform air gap.
- A thick film of Benzocyclobutene (BCB) low-k polymer ($k=2.65$) was used as an insulating layer to
 1. Reduce the parasitic capacitances and increase the motor efficiency.
 2. Reduce wafer curvature (compared to SiO_2) due to low residual stress.

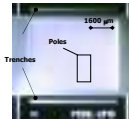
- The stator fabrication process comprises of three BCB deposition, two metal deposition steps, and a deep reactive ion etching (DRIE) step.
- The slider fabrication process comprises a DRIE step for fabricating poles and trenches.



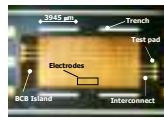
Schematic 3D view of the B-LVCM.

Parameter	Value
Electrode pole width, μm	90/90
Electrode pole pitch, μm	120/180
Electrode pole number	84/36
Air gap, μm	26-34
Microball diameter, μm	284.5
Trench width, μm	290
Microball material	440C stainless steel

Micromotor geometry specifications.



Optical micrograph (top-view) of the slider.



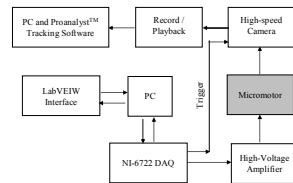
Optical micrograph (top-view) of the 6-phase stator.

CHARACTERIZATION

Dynamic characterization of the 6-phase B-LVCM is performed to obtain instantaneous velocity, acceleration, net force, and friction coefficient from the displacement measurement.

(a) Test Setup

- The micromotor test station comprises the following units
 - Six-channel, high-voltage actuation
 - Low noise, monochromic, high-speed video camera: 1000 frames-per-second (fps)
 - Image processing and tracking



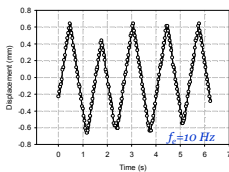
Block diagram of the micromotor test station.

(b) Displacement Measurement at 30 fps

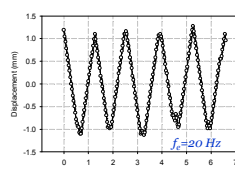
- Position of the slider is measured versus time.
- The average velocity is measured from the slope of the graphs.
- The predicted average velocity of the slider is given by $V_{avg} = 2Wf_e$ where W is the width of the electrode and f_e is the frequency of the excitation voltage.

Excitation frequency (Hz)	Predicted average velocity (mm/s)	Measured average velocity (mm/s)
10	1.80	1.91±0.02
20	3.60	3.98±0.02
40	7.20	7.37±0.12
80	14.40	7.21-11.10

Comparison of predicted and measured average velocity



Displacement of the slider when excited by 120V, six-phase, square pulses

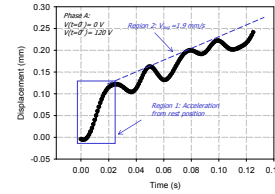


- The results show a good agreement between the predicted and measured values for the average velocity for $f_e \leq 60\text{Hz}$.

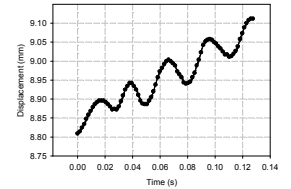
CHARACTERIZATION

(C) Transient Response Measurement at 635-1000 fps

- Transient response of the micromotor to 120-V square pulses was measured using high-speed camera system.
- Micromotor has a second-order step response modeled as a damped sinusoidal function.

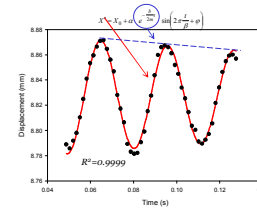


Startup of the micromotor from rest position captured at 1000 fps.

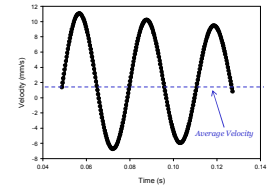


Position of the slider, $X(t)$, in 130-ms time window captured at 635 fps.

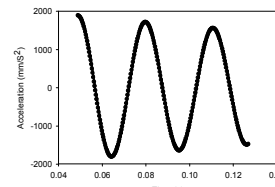
- Velocity and acceleration of the slider were calculated from the first and second derivatives of the displacement data, respectively.
- Instantaneous net force on the 0.1-gram slider was calculated to be 0.19 mN in amplitude.
- The micromotor was modeled as a mass-dashpot-spring system where m is the mass of the slider, b is the dashpot coefficient representing the friction of microballs and silicon housing, and k is the spring constant of the electrode-pole variable capacitance.
- The differential equation describing such a system is given by $m\ddot{x} + b\dot{x} + kx = 0$ (1)
- Dashpot coefficient was found to be $b=6.25 \times 10^{-4}$ Kg/s (at $V=120\text{V}$ and $f_e=10\text{Hz}$).



Local slider displacement, $X(t) = V_{avg} \cdot t$, showing damped sinusoidal transient response captured at 635 fps.



Instantaneous velocity of the slider.



Instantaneous acceleration and the net force of the slider.

DE: $m\ddot{x} + b\dot{x} + kx = 0$

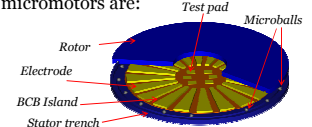
Solution: $x(t) = e^{-\frac{b}{2m}t} C \sin(\omega_d t + \phi)$



Mass-dashpot-spring model for the B-LVCM.

SUMMARY AND FUTURE WORK

- The dynamic characterization of a 6-phase, bottom-drive, linear, variable-capacitance micromotor (B-LVCM) supported on microball bearing was presented.
- The motion of the micromotor was captured using a high-speed video camera.
- Instantaneous velocity (11 mm/s), acceleration (1.9 mm/s²), and net force (0.19 mN) (all in amplitude) were measured.
- The motor was modeled with a mass-dashpot-spring system and dashpot coefficient was measured to be $b=6.25 \times 10^{-4}$ Kg/s.
- **Future work: Design, fabrication, and characterization of a rotary variable-capacitance micromotor supported on microball bearings.**
- Advantages of the proposed design to other rotary micromotors are:
 1. microball bearings support: reliable
 2. BCB electrical isolation: highly efficient
 3. Bottom-drive design: large active area and torque
 4. Wide variety of applications



Schematic 3D view of the rotary micromotor

ACKNOWLEDGEMENTS

This research was funded by Army Research Office through MURI Program under Grant No. ARMY-W911NF0410176, with Dr. Tom Doligalski as the technical monitor, the Army Research Lab under Grant No. CA#W911NF-05-2-0026, and the National Science Foundation under Grant No. ECS-0224361. The authors would like to thank Nitta Hass Company, Japan for providing the CMP supplies.